RST1 and RIPR connect the cytosolic RNA exosome to the Ski complex in *Arabidopsis*

Heike Lange*†[1], Simon Y. A. Ndecky[1], Carlos Gomez-Diaz[1], David Pflieger[1], Nicolas Butel[2], Julie Zumsteg[1], Lauriane Kuhn[3], Christina Piermaria[3], Johana Chicher[3], Michael Christie[4], Ezgi S. Karaaslan, Patricia L. M. Lang[4], Detlef Weigel[4], Hervé Vaucheret[2], Philippe Hammann[3] and Dominique Gagliardi*†[1]

[1]IBMP, CNRS, Université de Strasbourg, Strasbourg, France
[2]Institut Jean-Pierre Bourgin, INRA, AgroParisTech, CNRS, Université Paris-Saclay, Versailles, France
[3]Plateforme protéomique Strasbourg Esplanade FR1589 du CNRS, Université de Strasbourg, Strasbourg, France.
[4]Max Planck Institute for Developmental Biology, Tübingen, Germany

*equal contributions
† correspondence should be addressed to
hlange@unistra.fr or dominique.gagliardi@ibmp-cnrs.unistra.fr
+333 67 15 53 66

Abstract

The RNA exosome is a key 3'-5' exoribonuclease with an evolutionarily conserved structure and function. Its cytosolic functions require the co-factors SKI7 and the Ski complex. Here we demonstrate by co-purification experiments that the ARM repeat protein RESURRECTION1 (RST1) and RST1 INTERACTING PROTEIN (RIPR) connect the cytosolic *Arabidopsis* RNA exosome to the Ski complex. *rst1* and *ripr* mutants accumulate RNA quality control siRNAs (rqc-siRNAs) produced by the post-transcriptional gene silencing (PTGS) machinery when mRNA degradation is compromised. The small RNA populations observed in *rst1* and *ripr* mutants are also detected in mutants lacking the RRP45B/CER7 core exosome subunit. Thus, molecular and genetic evidence supports a physical and functional link between RST1, RIPR and the RNA exosome. Our data reveal the existence of additional cytosolic exosome co-factors besides the known SKI subunits. RST1

is not restricted to plants, as homologues with a similar domain architecture but unknown function exist in animals, including humans.

The main 3'- 5' exoribonucleolytic activity in eukaryotic cells is provided by the RNA exosome. It consists of a core complex composed of nine subunits (Exo9), to which the exoribonucleases RRP6 and DIS3/RRP44 differentially associate within the nucleolus, nucleoplasm or cytosol[1–4]. Whilst the overall structure and function of the RNA exosome is conserved, both the composition and enzymatic activities of exosome complexes vary among organisms. For example, most non-plant Exo9s including those in yeast and human are catalytically inactive[5], whereas plant Exo9s have retained a phosphorolytic activity originating from its prokaryotic ancestor[6]. This unique phosphorolytic activity of plant Exo9 acts in combination with the hydrolytic activities provided by RRP6 and DIS3[6]. Another exception among RNA exosomes is the association of human Exo9 with functionally distinct DIS3L and DIS3 proteins, only the latter of which is conserved in yeast and plants[3,7].

In all eukaryotes investigated, the catalytic activities of the RNA exosome are modulated by cofactors that aid in the recognition of specific types of substrates and that couple exosome-mediated degradation to cellular processes such as ribosome biogenesis or mitosis[8–15]. All "activator-adapter" or "exosome targeting" complexes that have been characterized to date contain an RNA helicase from the MTR4/SKI2 family as a central component. In addition, exosome targeting complexes typically comprise RNA binding proteins, non-canonical poly(A) polymerases or factors mediating protein-protein interactions.

Most exosome targeting complexes described to date are nuclear. They include the TRAMP (TRF4-AIR1-MTR4 polyadenylation) complexes in both baker's yeast and humans[16–19], the human PAXT (polyA tail exosome targeting) complex[22], the NEXT (nuclear exosome targeting) complexes that differ slightly in humans and plants[19,23] and the MTREC (Mtr4-like 1 (Mtl1)-Red1-core) complex in fission yeast[24,25]. These MTR4 containing complexes assist the exosome in nuclear RNA surveillance by targeting various RNA substrates, including precursors of ribosomal and other non-coding RNAs, spurious transcripts generated by pervasive transcription and untimely, superfluous or misprocessed mRNAs[17,19,23,24,26–30].

In remarkable contrast to the diversity of nuclear exosome cofactors, a single conserved protein complex, the Superkiller (Ski) complex, is known to assist the exosome in the cytosol.

The Ski complex consists of the MTR4-related RNA helicase SKI2, the tetratricopeptide repeat protein SKI3 and two copies of the WD40-repeat protein SKI8[31–33]. Association of the Ski complex with the exosome core complex requires an additional protein, SKI7[34]. In yeast, the genes encoding Ski7 and Hbs1, which binds to Dom34 (PELOTA in humans and plants) for the release of stalled ribosomes[35], arose from a whole genome duplication event. In other eukaryotes including mammals and plants, the SKI7 and HBS1 proteins are produced by alternative splicing from a single locus[36–38].

The Ski complex is conserved in *Arabidopsis thaliana*[39], but its physical association with the exosome core has not been investigated yet. An initial experiment to affinity-capture factors associated with the *Arabidopsis* exosome identified the homologue of DIS3 and two nuclear RNA helicases, AtMTR4 and its closely related homologue HEN2[23]. In addition, *Arabidopsis* Exo9 systematically co-purified with a 1840 amino acid ARM repeat protein of unknown molecular function named RESURRECTION 1 (RST1)[23]. RST1 was originally identified in a genetic screen for factors involved in the biosynthesis of epicuticular waxes[40]. Epicuticular waxes are a protective layer of aliphatic very long chain (VLC) hydrocarbons that cover the outer surface of land plants[41,42]. *rst1* mutants have less wax on floral stems than wild-type plants, and about 70% of the seeds produced by *rst1* mutants are shrunken due to aborted embryogenesis[40]. The molecular function of RST1 remains unknown. Interestingly, one of the two RRP45 exosome core subunits encoded in the *Arabidopsis* genome, named RRP45B or CER7 (for ECERIFERUM 7) was also identified in a genetic screen aimed at identifying enzymes or regulators of wax biosynthesis[43]. The wax-deficient phenotype of *rrp45b*/*cer7* mutants (*cer7* from now on) is suppressed by mutations in genes encoding RNA silencing factors such as RDR1, RDR6, AGO1, SGS3 and DCL4[44,45]. This and the identification of small RNAs accumulating in *cer7* mutants revealed that the wax deficiency observed in *cer7* plants is due to post-transcriptional silencing of *CER3* mRNAs[44,45], encoding a protein that together with the aldehyde decarbonylase CER1 catalyses the synthesis of VLC alkanes from VLC acyl-CoAs[46,47]. These results demonstrated that the RNA exosome contributes to the degradation of the *CER3* mRNA and that the wax-deficient phenotype of *cer7* mutants is a consequence of the established link between RNA degradation and silencing pathways[44,45,48]. Indeed, in plants, the two major exoribonucleolytic pathways that degrade RNAs either from 5' to 3' or from 3' to 5' also prevent that degradation intermediates such as uncapped or RISC-cleaved mRNAs are attacked by post-transcriptional gene silencing (PTGS)[49–54], a mechanism required for the destruction of non-self RNAs originating from viruses or transgenes[55].

Here, we demonstrate by multiple reciprocal co-purification assays coupled to mass spectrometry analyses that the *Arabidopsis* exosome core complex Exo9 associates with the ARM repeat protein RST1, SKI7, another protein that we named RIPR (for RST1 interacting protein) and the SKI complex. Our data show that RST1 and RIPR suppress the silencing of transgenes as well as the production of secondary siRNAs from endogenous exosome targets such as RISC cleaved transcripts and certain endogenous mRNAs which are prone to PTGS. Those mRNAs include the *CER3* mRNAs explaining that the *rst1* and *ripr* mutants share the *cer7* wax deficiency phenotype. Taken together, our biochemical and genetic data establish RST1 and RIPR as cofactors of the cytoplasmic exosome and the Ski complex in plants.

Results

Wax deficiency in *rst1* mutants is caused by *CER3* silencing

To investigate whether the wax deficiency of *rst1* plants is linked to compromised degradation of the *CER3* mRNA as reported in *cer7* mutants[43], we compared the stems of wild-type and mutant plants grown under identical conditions. Due to the light reflecting properties of the wax crystals that cover the outer cuticle, stems of wild type *Arabidopsis* plants appear whitish (or bluish in cold light, Fig. 1A). Consistent with previous reports, plants lacking the exosome core subunit RRP45A have whitish stems signifying intact wax biosynthesis[43]. By contrast, plants with T-DNAs inserted in the *RRP45B*/*CER7* (*AT3G60500*) and *RST1* (*AT3G27670*) loci have glossy green stems indicating wax deficiency[40,43] (Fig. 1A). Gas chromatography followed by mass spectrometry (GC-MS) analysis of extracts obtained from the stem surface confirmed that the amounts of the VLC derivatives nonacosane, 15-nonacosanone, and 1-octacosanol, three major components of epicuticular stem wax in *Arabidopsis*, were similarly reduced in *cer7* and in *rst1* mutants (Fig. 1B). Ectopic expression of RST1 fused to GFP in *rst1-3* plants restored the biosynthesis of nonacosane, 15-nonacosanone and 1-octacosanol and resulted in wild type-like whitish stems (Fig. 1A,B). Previous studies established that the wax deficiency of *cer7* mutants is due to post-transcriptional silencing of the mRNA encoding *CER3*[43–45,48], a subunit of a VLC alkane-forming complex[46,47]. Indeed, RNA blots revealed a severe reduction of the *CER3* mRNA and an accumulation of *CER3*-derived small RNAs in both *cer7* and *rst1* mutants (Fig 1C). Mutating the PTGS factor SUPPRESSOR OF GENE SILENCING 3 (SGS3) in *rst1-2* plants abolished the production of *CER3*-derived small RNAs, restored wild-type levels of the *CER3* mRNA and allowed the production of epicuticular wax as demonstrated in the *rst1 sgs3*

double mutant (Fig. 1D). These results show that the wax-deficient phenotype of *rst1* mutants is caused by silencing of the *CER3* mRNA, as reported for *cer7* mutants.

RST1 is a suppressor of transgene silencing

Two independent genetic screens identified *rst1* point mutations as suppressors of silencing. The first screen aimed to identify mutations suppressing the phenotype of *MIM156* plants. *MIM156* plants express an artificial non-coding RNA with an uncleavable miRNA 156 recognition site[56]. Ectopic expression of this miRNA target mimicry (MIM) construct reduces both levels and activity of endogenous miR156 and leads to a characteristic phenotype with spoon-shaped cotyledons, prematurely serrated rosette leaves and a reduced leaf initiation rate during vegetative growth (Fig. 2A). *MIM156 rst1-4* plants were recovered from an EMS-treated population of *MIM156* plants that had been visually screened for restoration of normal growth and development. *MIM156 rst1-4* plants display the spoon-shaped cotyledons of the parental line but wild type-like leaf initiation rates and rosette leaf serration. We mapped the suppressor mutation by whole genome sequencing to the *RST1* gene and specifically the G3118A mutation causing a G706D amino acid change (Fig. 2B). Expressing a genomic *RST1* construct in *MIM156 rst1-4* plants restored the MIM156 phenotype confirming that the *rst1-4* mutation was responsible for the suppressor effect (Fig. 2A). We then tested the accumulation of *CER3*-derived siRNAs in this novel *rst1* allele. As compared to the T-DNA insertion alleles *rst1-2* and *rst1-3*, *rst1-4* mutants accumulated lower levels of *CER3*-derived siRNAs, indicating that *rst1-4* is a weak allele (Fig. 2C). Next, we analysed the accumulation of both the full length *MIM156* non-coding RNA and *MIM156*-derived siRNAs by RNA blots. This experiment revealed low levels of *MIM156*-derived siRNAs in the parental *MIM156* line indicating that the *MIM156* transcript is spontaneously targeted by PTGS, as often observed with highly expressed transgenes. Compared to the parental line, *MIM156 rst1-4* plants had reduced levels of the full-length *MIM156* transcript but accumulated increased levels of *MIM156* derived siRNAs (Fig. 2D). The increased accumulation of these siRNAs in the *MIM156 rst1-4* suggests that RST1 restricts the production of *MIM156*-derived siRNAs, which prevents complete destruction of the full-length transcript by PTGS.

The second screen directly aimed at identifying factors affecting the posttranscriptional silencing of the *35Sprom:GUS* transgene in the reporter line *L1 jmj14-4* [57]. This screen identified *rst1-5,* a C4824T mutation in *RST1* resulting in a truncation of the RST1 protein (Q1010*) (Fig. 2B). Compared to the *L1 jmj14-4* parental line, *L1 jmj14-4 rst1-5* plants had decreased levels of *GUS* mRNA and increased levels of *GUS*-derived siRNA

(Fig 2E). This result resembled the effects of *rst1-4* on the accumulation of *MIM156* transcript and *MIM156* derived siRNAs (Fig. 2D). Backcrossing *L1 jmj14-4 rst1-5* to wild type yielded *rst1-5* plants, which showed a pronounced accumulation of *CER3*-derived siRNA similar to *rst1-2* and *rst1-3* (Fig. 2C). To further demonstrate that *rst1-5* enhances PTGS, we introduced the *rst1-5* mutation into the well-established reporter lines *6b4* and *Hc1*[57] (Fig. 2F). These lines harbour the same *35S:GUS* transgene as the *L1 jmj14-4* line, but inserted at different locations in the *Arabidopsis* genome. In a wild-type background, line *6b4* does not trigger sense transgene PTGS (S-PTGS), while line *Hc1* triggers S-PTGS in 20% of the population (Fig. 2F). In genetic backgrounds having impaired RNA degradation, both Hc1 and 6b4 lines trigger S-PTGS at increased frequencies, which provides a quantitative readout[23,49–51,53,58]. 86% of the 6b4 *rst1-5* plants and 100% of the Hc1 *rst1-5* plants triggered silencing of the *35S:GUS* reporter (Fig. 2F). This result confirmed that RST1 functions as a suppressor of S-PTGS comparable to other proteins involved in RNA degradation[23,49–51,53,58] .

RST1 co-purifies with the exosome, SKI7 and RIPR

To examine the intracellular distribution of RST1, we used a *rst1-3* mutant line expressing RST1 proteins fused to GFP at its N- or C-terminus. Both fusion proteins were functional as they rescued the wax deficiency of *rst1-3* (Fig. 1), and showed a diffuse cytoplasmic distribution in root cells of stable *Arabidopsis* transformants similar to the cytoplasmic marker protein PAB2 (Fig. 3). Therefore we conclude that RST1 is a cytoplasmic protein, which is in contrast to a previous study, which had proposed that RST1 is localized at the plasmamembrane[59]. In our previous experiments, RST1 co-purified with Exo9 using the core exosome subunit RRP41 as bait[23]. To verify the association of RST1 with Exo9 we used GFP-RST1 or RST1-GFP as baits for immuno-precipitation (IP) experiments followed by LC-MS/MS analyses (15 IPs). Indeed, among the proteins that were enriched in RST1 IPs were the nine canonical subunits of Exo9: CSL4, MTR3, RRP4, RRP40A, RRP41, RRP42, RRP43, RRP45B/CER7 and RRP46 (Fig. 4A, Supplementary Table 1). By contrast, we did not detect HEN2 or MTR4, the two main cofactors of nucleoplasmic or nucleolar exosomes, respectively. The lack of HEN2 and MTR4 detection is in agreement with the cytoplasmic localization of RST1. Noteworthy, RST1 co-purified with the cytoplasmic protein encoded by *AT5G10630*, the mRNA of which is alternatively spliced to produce either HBS1 or SKI7 proteins. As compared to the *HBS1* mRNA, the *SKI7* mRNA contains an additional exon encoding the putative exosome interaction domain of the *Arabidopsis* SKI7 protein[38]. Inspection of the peptides detected in the RST1 IP revealed the presence of peptides specific

to the SKI7 splice isoform (Supplementary Fig. S1). This and the fact that SKI7 proteins are bound to yeast and human exosome complexes indicate that the *AT5G10630* gene product which co-purified with RST1 is indeed SKI7 rather than HBS1. The three components of the cytoplasmic Ski complex were also detected in RST1 IPs, albeit their enrichment relative to control IPs did not pass the $p<0.05$ threshold. Together, these IP results support the exclusively cytoplasmic localisation of RST1 and confirm its interaction with the Exo9 core complex. Furthermore, a protein of unknown function encoded by *AT5G44150* and that we termed RIPR for RST1 interacting protein, was the most enriched protein in all RST1 IPs (Fig. 4A).

Because our previous purifications of *Arabidopsis* exosome complexes with tagged RRP41 as bait were analysed using an older and less sensitive mass spectrometer[23], we repeated the experiment using the same experimental settings as we used for the RST1 IPs (6 IPs, Fig. 4B, Supplementary Table 2). This new experiment as bait confirmed the previously reported co-purification of the conserved exoribonuclease RRP44 and the two nuclear RNA helicases MTR4 and HEN2 with Exo9 and reproduced the co-purification of RST1. In addition, the new experiment revealed a significant enrichment of both RIPR and SKI7 in the RRP41 IPs.

Peptides specific to the alternative subunit RRP45A were present in the RRP41 IPs but absent when RST1 was used as bait, suggesting that RST1 may preferentially interact with CER7 (aka RRP45B)-containing exosome complexes. To test this hypothesis, we stably expressed GFP-tagged RRP45A and RRP45B/CER7 in *Arabidopsis* (Supplementary Fig. 2). Indeed, both RST1 and SKI7 were significantly enriched with CER7 as bait (Fig. 5, Supplementary Table 3). By contrast, RST1 and RIPR were not detected when RRP45A was used as bait, even though RRP45A and CER7 are both present in cytosolic and nuclear compartments, and notwithstanding that the large number of RRP45A IPs (14 IPs) was sufficient to detect the nuclear RNA helicase HEN2 and exoribonuclease RRP44, whose association to Exo9 is rather labile in *Arabidopsis*. These results indicate that RST1 and RIPR are bound to Exo9 with RRP45B/CER7 subunits, but not to Exo9 complexes that contain the alternative subunit RRP45A. In order to confirm the physical association of RIPR with RST1, we used RIPR with GFP-tags at either the N- or the C-terminal ends as bait in co-purification experiments (4 IPs, Fig. 6, Supplementary Table 4). RST1 was the most enriched protein in RIPR IPs. The nine subunits of the exosome were also detected but were less enriched than in the IPs with RST1 as bait (compare Fig. 4 and 6). By contrast, SKI7 as well as the three components of the Ski complex SKI2, SKI3 and SKI8 were amongst the most significantly enriched proteins co-purifying with RIPR (Fig. 6).

Altogether, the multiple reciprocal IPs confirm the interaction of RST1 with CER7-containing exosome core complexes and identify SKI7 and RIPR as additional binding partners of both RST1 and Exo9. Furthermore, our data indicate that RIPR bridges the association of RST1-SKI7 with the Ski complex.

Loss of RIPR function phenocopies *rst1* mutants

RIPR is conserved among flowering plants but has no clear sequence homologs in mosses, green algae or outside of the green lineage. RIPR is a 356 amino acid protein that lacks obvious functional domains and motifs or sequence homologies to known proteins. Confocal microscopy of *Arabidopsis* roots stably expressing RIPR-GFP fusion proteins revealed a diffuse cytoplasmic distribution (Fig. 7A) similar to the intracellular distribution of RST1 (Fig. 3). Because T-DNA insertion mutants in the *AT5G44150* locus were not available in *Arabidopsis* stock centres, we obtained two independent mutants using a CRISPR-Cas9 strategy. The mutants, named *ripr(insT)* and *ripr(insC),* had single T or C nucleotides inserted at position 179, creating premature stop codons 60 and 65 amino acids after the start codon, respectively (Fig. 7B, C, Supplementary Fig. S3). Interestingly, *ripr(insT)* and *ripr(insC)* mutant plants have glossy green stems resembling the stems of *rst1* and *cer7* plants (Fig. 7D). Moreover, about 70% of the seeds produced by *ripr(insT)* and *ripr(insC)* plants were shrunken, similar to the proportion of unviable seeds produced by *rst1-2*, *rst1-3* or *cer7-3* plants (Fig. 7E)[40]. RNA blots confirmed that the wax deficient phenotype of *ripr(insT)* and *ripr(insC)* is due to the accumulation of *CER3*-derived small RNAs and silencing of the *CER3* mRNA (Fig. 7F). Those results demonstrate that RIPR can, like RST1, suppress the production of small RNAs from the *CER3* locus. Finally, 56 /56 Hc1 *ripr(insT)* plants triggered silencing of the GUS PTGS reporter (Fig. 7G), demonstrating that RIPR also supresses transgene silencing. Taken together, loss of RIPR induced very similar physiological and molecular phenotypes as loss of RST1 or the exosome subunit CER7.

Small RNAs produced from endogenous mRNAs accumulate in *cer7*, *ripr* and *rst1* mutants

The association of RST1 and RIPR with the exosome complex and the fact that loss of RST1 or RIPR phenocopies the *cer7* mutation suggested that both RST1 and RIPR are involved in the exosome-mediated degradation of the *CER3* mRNA before it can become a template for the production of *CER3*-derived small RNAs. To identify other common targets of RST1, RIPR and the exosome complex we analysed small RNA libraries prepared from wild-type

plants and from *cer7*, *rst1* and *ripr mutants* (Fig. 8A). This analysis identified more than 300 mRNAs that gave rise to small RNAs in *cer7* (Supplementary Table 5), including 5 of the 6 mRNAs that were previously shown to undergo silencing in absence of the RRP45B/CER7 exosome subunit[45]. Many of the loci that generate small RNAs in *cer7* mutants have previously been shown to produce siRNAs in *ski2* single mutants, *ski2 xrn4* double mutants or in the decapping mutants *dcp2* and *vcs*[51,52,54], and/or are known or predicted targets of miRNAs (Supplementary Table 5). Because these siRNAs are produced from protein coding genes in RNA degradation mutants, they have been termed ct-siRNAs (coding-transcript siRNAs) or rqc-siRNAs (RNA quality control siRNAs)[51,52,54]. About one third of the loci that generated rqc-siRNA in *cer7* mutants produced significant amounts of rqc-siRNAs in *rst1* and *ripr* mutants as well, while only very few loci were specifically observed in only *ripr* or *rst1* (Fig. 8B*)*. The observation of quasi identical populations of small RNAs in *rst1* and *ripr* and the fact that almost all loci affected by *rst1* or *ripr* are also affected in *cer7* strongly support the conclusion that RST1 and RIPR are required for the degradation of at least a subset of cytoplasmic exosome targets.

Discussion

This study identifies RST1 and RIPR as two previously unknown co-factors which support the function of the cytoplasmic RNA exosome in *Arabidopsis*. Three lines of evidence back our conclusion. Firstly, RST1 and RIPR are physically associated with the exosome core complex and the Ski complex, respectively, both of which act together in the degradation of cytoplasmic RNAs. Secondly, both RST1 and RIPR suppress the silencing of a transgenic reporters similar to almost all known main RNA degradation factors including proteins involved in decapping, the 5'-3' exoribonucleases XRN3 and XRN4, and both subunits of Exo9 and Exo9 cofactors involved in 3'-5' RNA degradation[23,49–51,53]. Thirdly, loss of function mutations of either RST1, RIPR or the exosome subunit CER7 lead to the accumulation of illegitimate siRNAs generated from endogenous protein-coding genes many of which have been previously found to produce siRNAs in *ski2*, *xrn4 ski2*, or in mutants of the decapping complex[51,52,54]

The current hypothesis for the production of rqc-siRNAs is that mRNA degradation intermediates such as decapped, deadenylated or cleaved mRNAs, including the fragments produced by RISC, must be rapidly eliminated to avoid that they serve as substrates for the synthesis of double-stranded RNA by endogenous RNA-dependent RNA polymerases and SGS3[49–52,54,60]. Likely, the largely redundant 5'-3' degradation by the cytoplasmic

exoribonuclease XRN4 and 3'-5' degradation by the cytoplasmic exosome and the Ski complex ensures the rapid elimination of mRNAs after their degradation has been initiated by decapping, deadenylation or RISC-mediated cleavage, thus preventing the production of rqc-siRNAs. Vice versa, accumulation of rqc-siRNAs indicates impaired RNA degradation. The fact that similar rqc-siRNA profiles are observed in *cer7*, *rst1* and *ripr* mutants indicates that CER7, RST1 and RIPR contribute to the degradation of an overlapping set of mRNA targets.

It is important to note that both the loci concerned and the levels of siRNAs from a given loci vary among plants of the same genotype and grown under identical conditions. Also, not each of the loci that give rise to rqc-siRNA undergoes silencing, i.e. full suppression of its expression[61]. Yet, PTGS is obviously consistently triggered for certain *Arabidopsis* mRNAs. For instance, compromising 3'-5' degradation leads to silencing of the *CER3* and few other mRNAs, while distinct loci appear to be more sensitive to impaired decapping or 5'-3' decay[51,52,54]. Interestingly, many of the mRNAs that reproducibly generate small RNAs in RNA degradation mutants including the *CER3* mRNA, have actually no sequence homology to miRNAs (Supplementary Table 5). It is therefore tempting to speculate that mRNAs prone to PTGS possess common intrinsic features that trigger the recruitment of SGS3 and RDR6. One of the currently discussed propositions is that highly expressed mRNAs are more likely to generate aberrant RNAs than moderately or low expressed ones[54]. In addition, certain mRNAs prone to RNA silencing may be cleaved by off-targeted RISC, or are perhaps substrates of other endonucleases. Alternatively, secondary structures or strong association to proteins may impede degradation by at least one of the otherwise largely redundant 5'-3' and 3'-5' degradation pathways and could explain why some mRNAs are more likely to become substrate for RNA-dependent RNA polymerases than mRNAs which are efficiently degraded from both directions. Yet, about 30% of the rqc-siRNAs generating loci in *rst1* and *ripr* are known or predicted miRNA targets (Supplementary Table 5). Hence, at least for those, the initial substrate for RDR6-dependent siRNA production could be a RISC-cleaved mRNA fragment. Since miRNAs and AGO1, the main effectors of RISC, are associated with polysomes[62,63], 5' cleavage products that could be generated by RISC on polysomes resemble truncated mRNAs without a stop codon and without a polyA-tail. Therefore, we can presume that RST1 and RIPR, together with the Ski complex and the RNA exosome, participate in the elimination of no-stop RNA. The notion that 5' RISC-cleaved fragments that fail to be degraded by RST1-RIPR-SKI and the exosome become a substrate for the production of small RNAs fits well with the observation that the full-length cleavage fragments of only 10-20% of the *Arabidopsis* miRNA targets can be detected in the no-stop decay mutant *pelota*[60].

Our data also have important implications on the physical organisation of the cytoplasmic RNA exosome and the Ski complex. In *Arabidopsis* and closely related species, two genes encode the exosome core subunit RRP45. *Arabidopsis* RRP45A and RRP45B/CER7 share 88% identity over their first 300 amino acids. Both subunits are located in cytosolic and nuclear compartments, and are at least in stable transformants, similarly enriched in nucleoli. Interestingly, both RST1 and RIPR only associated with RRP45B/CER7-containing exosomes, while no peptide of RST1 was detected in any of the fourteen experiments that we performed using RRP45A as bait. Instead, RRP45A-containing exosomes preferentially co-purified with the nuclear RNA helicase HEN2, in line with previous results obtained using HEN2 as bait[23]. Our results indicate that RST1 preferentially associates with the CER7-containing version of the *Arabidopsis* exosome. Compared to RRP45A, CER7 possesses an extra C-terminal domain of 135 aminoacids, which may be important for the recruitment of RST1. However, a previous study suggested that these extra amino acids are dispensable for the function of CER7 in the degradation of the *CER3* mRNA[43]. Moreover, the ectopic expression of RRP45 in *cer7* mutants rescued their wax-deficient phenotype[43]. A possible explanation is that overexpression of RRP45A allows a weak interaction with RST1 that is below the detection level in our IPs with RRP45A as bait. An alternative explanation could be that the physical interaction between RST1 and Exo9 is not essentially required for the function of both proteins in the turnover of the *CER3* mRNA.

The observation that RST1 is among the most enriched proteins captured with either RRP41 or CER7 as bait suggests that RST1 is stably associated with the exosome core complex. The strong enrichment of both RIPR and SKI7 with RST1 as bait and the observation that the Ski complex purifies mainly with RIPR suggests that RST1 and RIPR link the exosome to the Ski complex in plants. Future experiments will address the possibility that RIPR may be required to link the Ski complex with the core exosome while RST1 could stabilize the binding of Exo9 and SKI7. Other interesting possibilities are that RST1 and/or RIPR affect the recognition of target RNAs or the recruitment of the exosome to ribosomes. In fact we do detect ribosomal proteins in the all of our IPs, but with low enrichment scores (Supplementary Tables 1-4, or explore the interactive volcano blots available on figshare https://doi.org/10.6084/m9.figshare.c.4483406). Whether this has a technical basis or truly reflects a poor association of Exo9-RST1-RIPR-Ski complex with ribosomes remains to be investigated. Interestingly, a recent study in yeast identified Ska1 as a protein that impedes the association of the yeast Ski-Exo9 complex with the ribosome[64]. Similar to RIPR in *Arabidopsis*, Ska1 affinity-captured the Ski complex. But unlike RST1 or RIPR, the Ska1-Ski

complex is not required for the degradation of coding regions, and instead, has a specific function in the elimination of RNAs devoid of ribosomes such as 3' UTRs or long non-coding RNAs. Apparently, overexpressing of Ska1 outcompetes the association of the Ski complex with ribosomes, suggesting that the association the Ski complex with either Ska1 or the ribosome is mutually exclusive[64]. Of note, sequence homologs of Ska1 seem to be restricted to *S. cerevisiae* and some closely related fungi, although proteins with similar functions may exist in other species.

RIPR seems to be conserved in flowering plants but is absent from the genomes of mosses and green algae, suggesting a relative recent evolutionary origin. By contrast, RST1 is deeply conserved in the green lineage. Moreover, a single ARM repeat protein comprising the same domain of unknown function DUF3037 (IPR022542) as RST1 is conserved in humans, across all metazoa and in ancient amoebozoa such as *Dictyostelium*, but is apparently absent from modern fungi (PTHR16212 protein family). The human DUF3037 protein KIAA1797 was named Focadhesin because its GFP fusion protein has been detected in focal adhesion points of astrocytoma cells[65]. Interestingly, a recently generated high-throughput dataset monitoring the migration of proteins in sucrose gradients with or without RNase treatment detected Focadhesin as a putative component of an RNA-dependent complex (Sven Diederichs lab, http://r-deep.dkfz.de/). More work is needed to fully understand the molecular function of human Focadhesin. It will be interesting to investigate whether Focadhesin is also associated with the function of the RNA exosome in animals.

Material and Methods

Plant material

Plants were grown on soil or *in vitro* on Murashige and Skoog medium supplemented with 0.5 % sucrose at 20°C in 16 h light and 8 h darkness. All plants were of the Col-0 accession, which served as wild type in all experiments. The T-DNA insertion lines *cer7-2* (Salk_003100), *cer7-3* (GK_089C02), *rrp45a* (GK_665D02), *sgs3-13* (Salk_039005) and *rst1-2* (Salk_070359), *rst1-3* (Salk_129280) have been described in [44,46] and [40], respectively. The *rst1-5* and *rst1-4* alleles are EMS alleles identified during this study. Starting point for the identification of *rst-5* was the EMS mutagenesis of the line *L1 jmj14-4* line in which PTGS of the *35Sprom:GUS* transgene inserted at the *L1* locus is partially impaired by the *jmj14-4* mutation[57,66]. The *rst1-4* mutant was identified following EMS treatment of *MIM156*[56]. EMS mutagenesis of seeds was performed as described in[67]. Mutations were identified by mapping-by-sequencing using pooled F2 plants exhibiting the phenotype of

interest. Sequencing libraries prepared with the Illumina TruSeq DNA Sample Preparation Kit were 10-plexed (Illumina adapters Set A) per flow-cell lane and sequenced on an Illumina HiSEquation 2000 instrument to obtain at least 10-fold genome coverage. The SHOREmap technique was used to identify SNPs and mapping intervals[68]. The EMS mutants were backcrossed to Col-0 to remove the *MIM156* transgene (rst1-4) or the *jmj14-4* mutation and the *L1 35Sprom:GUS* reporter (*rst1-5*). Presence or absence of the transgenes and mutations were confirmed by PCR genotyping.

PTGS analysis

Hc1 rst1-5, *Hc1 ripr(insT)* and *6b4 rst1-5* plants were obtained by crosses. S-PTGS frequencies were assessed by GUS activity assays as described previously[69].

CRISPR-Cas9 editing of *AT5G44150*

The target site at position +179 from the ATG of the *AT5G44150* gene was selected using the CRISPR plant webtool (http://www.genome.arizona.edu/crispr/CRISPRsearch.html). No off-targets were predicted for the guide RNA TCATACCGATCCCAATT'CGA targeting the complementary strand at Chr5:17764907-17764927. 100 pmol of the oligonucleotides 5'-ATTGTCATACCGATCCCAATTCGA-3' and 5'-AAACTCGAATTGGGATCGGTATGAC-3' were phosphorylated for 30 min at 37 °C using 1 mM ATP and 1 unit polynucleotide kinase (NEB) in the buffer supplied by the manufacturer and then hybridized in a thermocycler (5 min 95 °C, cooling rate 5 °C/min, 5 min 25 °C). 100 fmol of hybridized oligonucleotides were ligated overnight at 18 °C to 10 ng of Aar1-digested and dephosphorylated vector pKI1.1R[70]. An aliquot of the ligation mixture was transformed in TOP10 *E. coli* cells (Invitrogen). The correct insertion of the guide RNA in the vector was confirmed by Sanger sequencing before plasmids were introduced in *Agrobacterium tumefaciens* strain GV3101 for the transformation of Col-0 plants by floral dip[71]. pKI1.1R's T-DNA confers a red fluorescence protein expressed under the seed-specific OLEO1 promoter. Fluorescent T1 seeds were selected using an epifluorescence-equipped binocular. Plants were genotyped by high resolution melting using the precision melt supermix (Biorad) in a Roche Lightcyler 480 and further confirmed by Sanger sequencing. Plants carrying an insertion at the *AT5G44150* target site were selfed and RFP-negative T2 seeds devoid of the Cas9-containing T-DNA were selected for outgrowth. Two independent T2 plants homozygous for the insertion of a single T or C at position +179 were selected for further characterization.

Expression of GFP-tagged fusion proteins

RRP41-GFP lines were made with constructs comprising the genomic sequence of *RRP41* including 1000bp upstream of the translation start site and were previously described in [6]. All other GFP-fusion proteins were expressed from the *UBIQUITIN 10* promoter. C-terminal fusion constructs contained the genomic sequence of the respective genes including the 5' UTR but lacking the Stop codon. For N-terminal fusions, the genomic sequences without the 5' UTR but including the 3' UTR were used. All sequences were amplified from genomic DNA, cloned into pENTR1a (Invitrogen) and transferred to pUBC-GFP and pUBN-GFP destination vectors[72], respectively, using Gateway^{R} recombinases. Expression vectors were transferred to *Agrobacterium* and used to transform *rst1-3* (for RST1-GFP and GFP-RST1), *cer7-2* for CER7-GFP, *rrp45a* for RRP45a-GFP, and Col-0 plants for both GFP-RIPR and RIPR-GFP.

Co-immunopurification experiments

Plants were selected by testing crude flower extracts by western blots using homemade antibodies specific to GFP. For each IP, 200-500 mg of flower buds pooled from at least 4 individual plants were ground in liquid nitrogen or directly in 2 ml ice-cold lysis buffer (50 mM Tris HCL pH 7.5, 25 or 50 mM NaCl, 1% Triton, protease inhibitors (Complete - EDTA, Roche). After removal of cell debris by centrifugation (2 times 5 min, 16000 x g, 4 °C) the cleared supernatants were incubated for 30 min with GFP antibodies coupled to magnetic microbeads (Miltenyi). Beads were loaded on magnetized MACS separation columns equilibrated with lysis buffer and washed 5 times with 300 µl washing buffer (50mM Tris HCL pH 7.5, 25 or 50 mM NaCl, 0,1 % Triton). Samples were eluted in 50 µl of pre-warmed elution buffer (Milteny). Control IPs were carried out with GFP antibodies in Col-0 or in plants expressing RFP or GFP alone. Additional control IPs were performed with antibodies directed against myc or HA epitopes.

Eluted proteins were digested with sequencing-grade trypsin (Promega) and analyzed by nanoLC-MS/MS on a QExactive+ mass spectrometer coupled to an EASY-nanoLC-1000 (Thermo-Fisher Scientific, USA) as described before[73]. Data were searched against the TAIR10 database with a decoy strategy. Peptides were identified with Mascot algorithm (version 2.5, Matrix Science, London, UK) and the data were imported into Proline 1.4 software (http://proline.profiproteomics.fr/). The protein identification was validated using the following settings: Mascot pretty rank <= 1, FDR <=1% for PSM scores, FDR <= 1% for

protein set scores. The total number of MS/MS fragmentation spectra was used to quantify each protein from at least two independent biological replicates. If not specified otherwise, biological replicates consisted of plants of the same genotype grown at different dates and in different growth chambers.

For the statistical analysis of the co-immunoprecipitation data we compared the data collected from multiple experiments for each bait against a set of 20 control IPs using a homemade R package as described in[73] except that the size factor used to scale samples were calculated according to the DESeq normalisation method (i.e. median of ratios method)[74]. The R-package performs a negative-binomial test using an edgeR-based GLM regression and calculates the fold change and an adjusted p-value corrected by Benjamini–Hochberg for each identified protein. The RST1 dataset comprised the data collected from 15 immunoprecipitation experiments performed in 6 biological replicates of each GFP-RST1 and RST1-GFP. 14 IPs from 4 biological replicates were performed with RRP45A. 6 experiments from 2 biological replicates were used for each of RRP41-GFP and CER7-GFP, and the RIPR dataset contained 4 IPs from 2 biological replicates of each RIPR-GFP and GFP-RIPR. Control IPs included 4 biological replicates of Col-0 incubated with GFP antibodies, 6 IPs from 4 biological replicates of GFP-expressing plants treated with GFP antibodies, and 10 IPs performed with anti-HA antibodies in 3 biological replicates RST1-GFP, 3 replicates GFP-RST1 and in 1 RFP sample. The mass spectrometry proteomics data have been deposited to the ProteomeXchange Consortium (http://proteomecentral.proteomexchange.org) via the PRIDE partner repository[75] with the dataset identifier PXD013435.

Epicuticular wax analysis

For each sample, 3 stem sections of 6 cm were immersed for 30 s in 10 ml chloroform. Extracts were dried under N2 gas, dissolved in 150 µl chloroform, transferred in an insert and again dried under N2 gas. Extracts were derivatized in a mix of BSTFA [*N,O* bis(trimethylsilyl) trifluoroacetamide) (> 99 %, Sigma)] / pyridine (> 99,5 %, sigma) (50/50, V/V) (1 h 80 °C with shaking at 300 rpm) before BSTFA-pyridine extracts were evaporated under N2 gas. The samples were dissolved in chloroform containing a mix of 9 alkanes (C10-C12-C15-C18-C19-C22-C28-C32-C36) as internal standards.

Derivatized silylated samples were analyzed by GC-MS (436-GC, Bruker; column 30-m, 0.25-mm, 0.25 µm; HP-5-MS) with He carrier gas inlet pressure programmed for constant flow of 1 ml/min and mass spectrometric detector (SCION TQ, Bruker; 70 eV, mass to charge ratio 50 to 800). GC was carried out with temperature-programmed injection at 50 °C over 2

min. The temperature was increased by 40 °C/min to 200 °C, held for 1 min at 200 °C, further increased by 3 °C/min to 320 °C and held for 15 min at 320 °C. Injector temperature was set to 230 °C with a split ratio of 3:1. Peaks in the chromatogram were identified based on of their mass spectra and retention indices. Mass spectra detected by GC-MS were compared with the spectra of known compounds stored in the National Institute Standard and Technology (NIST) and in the Golm Metabolome databases. Nonacosane, 15-nonacosanone and 1-octacosanol were identified with match values of 933, 865 and 952, respectively. Mass spectrometric detector peak areas were used for relative quantification with octacosane as internal standard.

RNA extractions and northern blots

RNA was extracted from the top 3 cm of inflorescence stems or from flowers with TRI-reagent (MRC) following the manufacturers instructions. After precipitation with 0.8 vol isopropanol for 1-3 h at -80 °C, RNAs were collected by centrifugation (30 min 16000 x g, 4 °C), washed twice with 70% EtOH, dissolved in water and further purified by adding 1 vol of Phenol:Chloroform:Isoamylalcohol (25:24:1). The aqueous phase was transferred in a fresh tube, RNAs were precipitated overnight with 2.5 vol of EtOH at -80 °C, collected by centrifugation, washed twice with 70 % EtOH and dissolved in water to approx. 2.5 µg/µl. For high molecular weight northern blots, 20 µg of total RNA were separated in a 2 % denaturing agarose gel containing 30 mM Tricine, 30 mM Triethanolamine and 40 mM Formaldehyde (4-6 h at 50 V). The RNA was blotted to Amersham Hybond-N+ membranes (GE Healthcare Life Sciences) and UV-crosslinked (254 nm). Membranes were stained with methylene blue and hybridized to ^{32}P radio-labeled DNA probes (DecaLabel, ThermoFischer) in PerfectHyb™ (Sigma) over night at 65 ºC. Sequences for primers used for amplification of probe templates are listed in Supplementary Table S6.

For low molecular weight and small RNA northern blots, 20 µg of total RNA were separated in 5% and 17 % polyacrylamide gels (19:1), respectively, containing 7 M Urea in 100 mM Tris, 100 mM Borate, 2 mM EDTA. RNA was transferred to Amersham Hybond-NX membranes (GE Healthcare Life Sciences) and either UV-crosslinked (LMW blots) or chemically crosslinked (small RNA blots) by incubation with 0.16 M l-ethyl-3-(3-dimethylaminopropyl) carbodiimide (EDC, Sigma) in 0.13 M 1-methylimidazole (Sigma), pH 8, for 1.5h at 60 °C. Membranes were hybridized to radio-labeled DNA probes overnight at 45 ºC. For loading controls, blots were stripped with boiling 0.1 % SDS, and hybridized to

a radiolabelled oligonucleotide specific to 7SL RNA, U6 snRNA or miR156. Oligonucleotide sequences are listed in Supplementary Table S6.

Microscopy

Plants were grown on MS agar plates supplemented with 0.5% sucrose. Roots from ten day-old seedlings were excised, placed with water under a coverslip and examined with a ZEISS LSM 780 confocal microscope.

small RNA libraries and analysis

RNA was prepared as described above from flower buds of 6 week-old plants. For each genotype, three biological replicates of Col-0 (wild type), *cer7-3*, *rst1-2*, *rst1-3*, *ripr(insT)*, *ripr(insC)* and two of *cer7-4* were grown at different dates in different growth chambers. Libraries were prepared from 1 µg of total RNA using the NEB Next Multiplex Small RNA Library Prep Set for Illumina (NEB #E7300S and #E7580S) following the manufacturer's instructions. After ligation of primers, cDNA synthesis and PCR amplification, pooled libraries were loaded on a NOVEX 6% polyacrylamide gel with 100 mM Tris, 100 mM Borate, 2 mM EDTA. Five fractions corresponding to 130-180 bp products were excised and eluted overnight in water. After EtOH precipitation, size and concentration of the fractions were checked with an Agilent 2100 Bioanalyzer (Agilent Technologies). The fraction of 140-150 bp containing the 21-22 nt small RNAs of interest was sequenced on a HiSeq 4000 sequencer (single-end mode 1x50bp).

Sequence reads were trimmed from 3'-adapters and low quality bases ($q < 30$) using cutadapt v1.18[76]. Reads were aligned without mismatches to the *Arabidopsis* TAIR10 genome using ShortStack v3.8.5[77] in unique mode (-u). Counts of 21 nt and 22 nt reads were extracted and annotated against TAIR10. Differential expression analysis was performed with DEseq2[78]. The data obtained from the two alleles of *cer7*, *rst1* and *ripr* were analysed together. Downstream analysis and data visualization were done with R. Only loci with log2FC > 1 and an adjusted p-value of < 0.01 were considered. PhasiRNA were identified with the help of ShortStack's phasing score (score >= 5). Potential miRNA target mRNAs were predicted using the psRNATarget webservice at (http://plantgrn.noble.org/psRNATarget)[79].

Statistical analysis

For the statistical analysis of proteomic and sequencing data, we used negative-binomial models based on the edgeR and DEseq2 packages, respectively, which calculate the fold change and adjusted p-values with a two-sided Wald test.

Gel and blot images

Uncropped blots and stem images are provided in Supplementary Figure S4.

Data availability.

The small RNAseq and mass spectrometry proteomics raw data that support the findings of this study have been deposited to the NCBI Gene Expression Omnibus (GEO) database, accession code GSE129736, and to the ProteomeXchange Consortium via the PRIDE[75] partner repository with the dataset identifier PXD013435, respectively.

Full resolution versions of all images, processed small RNA-seq data and interactive volcano blots are available at figshare (https://doi.org/10.6084/m9.figshare.c.4483406).

References

1. Lykke-Andersen, S., Tomecki, R., Jensen, T. H. & Dziembowski, A. The eukaryotic RNA exosome: same scaffold but variable catalytic subunits. *RNA Biol.* **8**, 61–66 (2011).
2. Wasmuth, E. V. & Lima, C. D. Exo- and endoribonucleolytic activities of yeast cytoplasmic and nuclear RNA exosomes are dependent on the noncatalytic core and central channel. *Mol. Cell* **48**, 133–144 (2012).
3. Tomecki, R. *et al.* The human core exosome interacts with differentially localized processive RNases: hDIS3 and hDIS3L. *EMBO J.* **29**, 2342–2357 (2010).
4. Schaeffer, D., Clark, A., Klauer, A. A., Tsanova, B. & van Hoof, A. Functions of the cytoplasmic exosome. *Adv. Exp. Med. Biol.* **702**, 79–90 (2011).
5. Dziembowski, A., Lorentzen, E., Conti, E. & Séraphin, B. A single subunit, Dis3, is essentially responsible for yeast exosome core activity. *Nat Struct Mol Biol* **14**, 15—22 (2007).
6. Sikorska, N., Zuber, H., Gobert, A., Lange, H. & Gagliardi, D. RNA degradation by the plant RNA exosome involves both phosphorolytic and hydrolytic activities. *Nat. Commun.* **8**, 2162 (2017).
7. Staals, R. H. J. *et al.* Dis3-like 1: a novel exoribonuclease associated with the human exosome. *EMBO J.* **29**, 2358–2367 (2010).
8. Schuller, J. M., Falk, S., Fromm, L., Hurt, E. & Conti, E. Structure of the nuclear exosome captured on a maturing preribosome. *Science* **360**, 219–222 (2018).
9. Falk, S. *et al.* Structural insights into the interaction of the nuclear exosome helicase Mtr4 with the preribosomal protein Nop53. *RNA N. Y. N* **23**, 1780–1787 (2017).
10. Yamashita, A. *et al.* Hexanucleotide motifs mediate recruitment of the RNA elimination machinery to silent meiotic genes. *Open Biol.* **2**, (2012).
11. Sugiyama, T. *et al.* Enhancer of Rudimentary Cooperates with Conserved RNA-Processing Factors to Promote Meiotic mRNA Decay and Facultative Heterochromatin Assembly. *Mol. Cell* **61**, 747–759 (2016).
12. Falk, S. *et al.* Structure of the RBM7–ZCCHC8 core of the NEXT complex reveals connections to splicing factors. *Nat. Commun.* **7**, (2016).
13. Andersen, P. R. *et al.* The human cap-binding complex is functionally connected to the nuclear RNA exosome. *Nat. Struct. Mol. Biol.* **20**, 1367–1376 (2013).
14. Vasiljeva, L., Kim, M., Terzi, N., Soares, L. M. & Buratowski, S. Transcription Termination and RNA Degradation Contribute to Silencing of RNA Polymerase II Transcription within Heterochromatin. *Mol Cell* **29**, 313—323 (2008).
15. Shah, S., Wittmann, S., Kilchert, C. & Vasiljeva, L. lncRNA recruits RNAi and the exosome to dynamically regulate pho1 expression in response to phosphate levels in fission yeast. *Genes Dev.* **28**, 231–244 (2014).
16. LaCava, J. *et al.* RNA degradation by the exosome is promoted by a nuclear polyadenylation complex. *Cell* **121**, 713—724 (2005).

17. Wyers, F. *et al.* Cryptic pol II transcripts are degraded by a nuclear quality control pathway involving a new poly(A) polymerase. *Cell* **121**, 725—737 (2005).
18. Vanacova, S. *et al.* A new yeast poly(A) polymerase complex involved in RNA quality control. *PLoS Biol* **3**, e189 (2005).
19. Lubas, M. *et al.* Interaction profiling identifies the human nuclear exosome targeting complex. *Mol. Cell* **43**, 624–637 (2011).
20. Schmidt, K. & Butler, J. S. Nuclear RNA Surveillance: Role of TRAMP in Controlling Exosome Specificity. *Wiley Interdiscip. Rev. RNA* **4**, 217–231 (2013).
21. Holub, P. & Vanacova, S. TRAMP Stimulation of Exosome. *Eukaryot. RNases Their Partn. RNA Degrad. Biog. Part A* **31**, 77–90 (2012).
22. Meola, N. *et al.* Identification of a Nuclear Exosome Decay Pathway for Processed Transcripts. *Mol. Cell* **64**, 520–533 (2016).
23. Lange, H. *et al.* The RNA helicases AtMTR4 and HEN2 target specific subsets of nuclear transcripts for degradation by the nuclear exosome in Arabidopsis thaliana. *PLoS Genet.* **10**, e1004564 (2014).
24. Egan, E. D., Braun, C. R., Gygi, S. P. & Moazed, D. Post-transcriptional regulation of meiotic genes by a nuclear RNA silencing complex. *RNA N. Y. N* **20**, 867–881 (2014).
25. Lee, N. N. *et al.* Mtr4-like protein coordinates nuclear RNA processing for heterochromatin assembly and for telomere maintenance. *Cell* **155**, 1061–1074 (2013).
26. Milligan, L., Torchet, C., Allmang, C., Shipman, T. & Tollervey, D. A nuclear surveillance pathway for mRNAs with defective polyadenylation. *Mol Cell Biol* **25**, 9996—10004 (2005).
27. Houseley, J., Kotovic, K., Hage, A. E. & Tollervey, D. Trf4 targets ncRNAs from telomeric and rDNA spacer regions and functions in rDNA copy number control. *EMBO J* **26**, 4996—5006 (2007).
28. Wang, S.-W., Stevenson, A. L., Kearsey, S. E., Watt, S. & Bühler, J. Global role for polyadenylation-assisted nuclear RNA degradation in posttranscriptional gene silencing. *Mol Cell Biol* **28**, 656—665 (2008).
29. Milligan, L. *et al.* A yeast exosome cofactor, Mpp6, functions in RNA surveillance and in the degradation of noncoding RNA transcripts. *Mol. Cell. Biol.* **28**, 5446–57 (2008).
30. Ogami, K. *et al.* An Mtr4/ZFC3H1 complex facilitates turnover of unstable nuclear RNAs to prevent their cytoplasmic transport and global translational repression. *Genes Dev.* **31**, 1257–1271 (2017).
31. Synowsky, S. A. & Heck, A. J. R. The yeast Ski complex is a hetero-tetramer. *Protein Sci. Publ. Protein Soc.* **17**, 119–25 (2008).
32. Halbach, F., Reichelt, P., Rode, M. & Conti, E. The yeast ski complex: crystal structure and RNA channeling to the exosome complex. *Cell* **154**, 814–826 (2013).
33. Schmidt, C. *et al.* The cryo-EM structure of a ribosome–Ski2-Ski3-Ski8 helicase complex. *Science* **354**, 1431–1433 (2016).
34. Araki, Y. *et al.* Ski7p G protein interacts with the exosome and the Ski complex for 3'-to-5' mRNA decay in yeast. *EMBO J.* **20**, 4684–4693 (2001).
35. Shao, S. *et al.* Decoding Mammalian Ribosome-mRNA States by Translational GTPase Complexes. *Cell* **167**, 1229-1240.e15 (2016).
36. Kalisiak, K. *et al.* A short splicing isoform of HBS1L links the cytoplasmic exosome and SKI complexes in humans. *Nucleic Acids Res.* **45**, 2068–2080 (2017).
37. Marshall, A. N., Han, J., Kim, M. & van Hoof, A. Conservation of mRNA quality control factor Ski7 and its diversification through changes in alternative splicing and gene duplication. *Proc. Natl. Acad. Sci. U. S. A.* **115**, E6808–E6816 (2018).
38. Brunkard, J. O. & Baker, B. A Two-Headed Monster to Avert Disaster: HBS1/SKI7 Is Alternatively Spliced to Build Eukaryotic RNA Surveillance Complexes. *Front. Plant Sci.* **9**, 1333 (2018).
39. Dorcey, E. *et al.* Context-Dependent Dual Role of SKI8 Homologs in mRNA Synthesis and Turnover. *PLoS Genet* **8**, e1002652 (2012).
40. Chen, X. *et al.* Mutation of the RESURRECTION1 locus of Arabidopsis reveals an association of cuticular wax with embryo development. *Plant Physiol.* **139**, 909–919 (2005).
41. Suh, M. C. *et al.* Cuticular Lipid Composition, Surface Structure, and Gene Expression in Arabidopsis Stem Epidermis. *Plant Physiol.* **139**, 1649–1665 (2005).
42. Wen, M. & Jetter, R. Composition of secondary alcohols, ketones, alkanediols, and ketols in Arabidopsis thaliana cuticular waxes. *J. Exp. Bot.* **60**, 1811–1821 (2009).
43. Hooker, T. S., Lam, P., Zheng, H. & Kunst, L. A core subunit of the RNA-processing/degrading exosome specifically influences cuticular wax biosynthesis in Arabidopsis. *Plant Cell* **19**, 904—913 (2007).
44. Lam, P. *et al.* RDR1 and SGS3, components of RNA-mediated gene silencing, are required for the regulation of cuticular wax biosynthesis in developing inflorescence stems of Arabidopsis. *Plant Physiol.* **159**, 1385–1395 (2012).
45. Lam, P. *et al.* The exosome and trans-acting small interfering RNAs regulate cuticular wax biosynthesis during Arabidopsis inflorescence stem development. *Plant Physiol.* **167**, 323–336 (2015).

46. Rowland, O., Lee, R., Franke, R., Schreiber, L. & Kunst, L. The CER3 wax biosynthetic gene from Arabidopsis thaliana is allelic to WAX2/YRE/FLP1. *FEBS Lett.* **581**, 3538–3544 (2007).
47. Bernard, A. *et al.* Reconstitution of Plant Alkane Biosynthesis in Yeast Demonstrates That Arabidopsis ECERIFERUM1 and ECERIFERUM3 Are Core Components of a Very-Long-Chain Alkane Synthesis Complex[C][W]. *Plant Cell* **24**, 3106–3118 (2012).
48. Zhao, L. & Kunst, L. SUPERKILLER Complex Components Are Required for the RNA Exosome-Mediated Control of Cuticular Wax Biosynthesis in Arabidopsis Inflorescence Stems. *Plant Physiol.* **171**, 960–973 (2016).
49. Gy, I. *et al.* Arabidopsis FIERY1, XRN2, and XRN3 are endogenous RNA silencing suppressors. *Plant Cell* **19**, 3451–61 (2007).
50. Moreno, A. B. *et al.* Cytoplasmic and nuclear quality control and turnover of single-stranded RNA modulate post-transcriptional gene silencing in plants. *Nucleic Acids Res.* **41**, 4699–4708 (2013).
51. Martínez de Alba, A. E. *et al.* In plants, decapping prevents RDR6-dependent production of small interfering RNAs from endogenous mRNAs. *Nucleic Acids Res.* **43**, 2902–2913 (2015).
52. Branscheid, A. *et al.* SKI2 mediates degradation of RISC 5'-cleavage fragments and prevents secondary siRNA production from miRNA targets in Arabidopsis. *Nucleic Acids Res.* **43**, 10975–10988 (2015).
53. Yu, A. *et al.* Second-Site Mutagenesis of a Hypomorphic argonaute1 Allele Identifies SUPERKILLER3 as an Endogenous Suppressor of Transgene Posttranscriptional Gene Silencing. *Plant Physiol.* **169**, 1266–1274 (2015).
54. Zhang, X. *et al.* Plant biology. Suppression of endogenous gene silencing by bidirectional cytoplasmic RNA decay in Arabidopsis. *Science* **348**, 120–123 (2015).
55. Voinnet, O. Use, tolerance and avoidance of amplified RNA silencing by plants. *Trends Plant Sci.* **13**, 317–328 (2008).
56. Todesco, M., Rubio-Somoza, I., Paz-Ares, J. & Weigel, D. A Collection of Target Mimics for Comprehensive Analysis of MicroRNA Function in Arabidopsis thaliana. *PLoS Genet.* **6**, (2010).
57. Le Masson, I. *et al.* Mutations in the Arabidopsis H3K4me2/3 demethylase JMJ14 suppress posttranscriptional gene silencing by decreasing transgene transcription. *Plant Cell* **24**, 3603–3612 (2012).
58. Hématy, K. *et al.* The Zinc-Finger Protein SOP1 Is Required for a Subset of the Nuclear Exosome Functions in Arabidopsis. *PLoS Genet.* **12**, e1005817 (2016).
59. Mang, H. G. *et al.* The Arabidopsis RESURRECTION1 Gene Regulates a Novel Antagonistic Interaction in Plant Defense to Biotrophs and Necrotrophs. *Plant Physiol.* **151**, 290–305 (2009).
60. Szádeczky-Kardoss, I. *et al.* The nonstop decay and the RNA silencing systems operate cooperatively in plants. *Nucleic Acids Res.* **46**, 4632–4648 (2018).
61. Sorenson, R. S., Deshotel, M. J., Johnson, K., Adler, F. R. & Sieburth, L. E. Arabidopsis mRNA decay landscape arises from specialized RNA decay substrates, decapping-mediated feedback, and redundancy. *Proc. Natl. Acad. Sci.* **115**, E1485–E1494 (2018).
62. Li, S. *et al.* Biogenesis of phased siRNAs on membrane-bound polysomes in Arabidopsis. *eLife* **5**, (2016).
63. Lanet, E. *et al.* Biochemical Evidence for Translational Repression by Arabidopsis MicroRNAs. *Plant Cell* **21**, 1762–1768 (2009).
64. Zhang, E. *et al.* A SKI subcomplex specifically required for the degradation of ribosome-free RNA regions. *bioRxiv* 409490 (2018). doi:10.1101/409490
65. Brockschmidt, A. *et al.* KIAA1797/FOCAD encodes a novel focal adhesion protein with tumour suppressor function in gliomas. *Brain J. Neurol.* **135**, 1027–1041 (2012).
66. Searle, I. R., Pontes, O., Melnyk, C. W., Smith, L. M. & Baulcombe, D. C. JMJ14, a JmjC domain protein, is required for RNA silencing and cell-to-cell movement of an RNA silencing signal in Arabidopsis. *Genes Dev.* **24**, 986–991 (2010).
67. Weigel, D. & Glazebrook, J. *Arabidopsis: A Laboratory Manual*. (CSHL Press, 2002).
68. Schneeberger, K. *et al.* SHOREmap: simultaneous mapping and mutation identification by deep sequencing. *Nat. Methods* **6**, 550–551 (2009).
69. Elmayan, T. *et al.* Arabidopsis mutants impaired in cosuppression. *Plant Cell* **10**, 1747–1758 (1998).
70. Tsutsui, H. & Higashiyama, T. pKAMA-ITACHI Vectors for Highly Efficient CRISPR/Cas9-Mediated Gene Knockout in Arabidopsis thaliana. *Plant Cell Physiol.* **58**, 46–56 (2017).
71. Clough, S. J. & Bent, A. F. Floral dip: a simplified method for Agrobacterium-mediated transformation of Arabidopsis thaliana. *Plant J. Cell Mol. Biol.* **16**, 735–743 (1998).
72. Grefen, C. *et al.* A ubiquitin-10 promoter-based vector set for fluorescent protein tagging facilitates temporal stability and native protein distribution in transient and stable expression studies. *Plant J. Cell Mol. Biol.* **64**, 355–365 (2010).
73. Chicois, C. *et al.* The UPF1 interactome reveals interaction networks between RNA degradation and translation repression factors in Arabidopsis. *Plant J. Cell Mol. Biol.* **96**, 119–132 (2018).
74. Anders, S. & Huber, W. Differential expression analysis for sequence count data. *Genome Biol.* **11**, R106

(2010).
75. Perez-Riverol, Y. *et al.* The PRIDE database and related tools and resources in 2019: improving support for quantification data. *Nucleic Acids Res.* **47**, D442–D450 (2019).
76. Martin, M. Cutadapt removes adapter sequences from high-throughput sequencing reads. *EMBnet.journal* **17**, 10–12 (2011).
77. Johnson, N. R., Yeoh, J. M., Coruh, C. & Axtell, M. J. Improved Placement of Multi-mapping Small RNAs. *G3 Bethesda Md* **6**, 2103–2111 (2016).
78. Love, M. I., Huber, W. & Anders, S. Moderated estimation of fold change and dispersion for RNA-seq data with DESeq2. *Genome Biol.* **15**, 550 (2014).
79. Dai, X., Zhuang, Z. & Zhao, P. X. psRNATarget: a plant small RNA target analysis server (2017 release). *Nucleic Acids Res.* **46**, W49–W54 (2018).

Author contribution

Study design, HL, DG; RNA analysis and co-purification experiments, HL, SYAN, CGD, PH, CP; Mass-spectrometry, PH, LK, JC; statistical analysis of co-IP data, HL; Gas-chromatography, JZ; Analysis of small RNA libraries, DP; *L1 jmj14-4* suppressor screen, mapping of *rst1-5*, RNA analysis Fig 2E, PTGS assays, NB and HV; MIM156 suppressor screen and mapping of *rst1-4*, MC, ESK, PLML and DW; Writing, HL, DG; Visualization, HL; Supervision, DG and HL; Funding Acquisition, DG.

Acknowledgments

We thank Nathalie Bouteiller for GUS assays, Ivan Le Masson for helping in the genetic screen that identified *rst1-5*, Sandrine Koechler for preparation of the small RNA library and Abdelmalek Alioua for high resolution melting analysis. Special thanks to Héléne Zuber for the R-script that enabled the statistical analysis of co-IP experiments. This work has been published under the framework of the LABEX ANR-10-LABX-0036_NETRNA and ANR-17-EURE-0023 and benefits from a funding from the state managed by the French National Research Agency as part of the Investments for the future program and the Centre National de la Recherche Scientifique. The funders had no role in study design, data collection and analysis, decision to publish, or preparation of the manuscript.

Competing financial interests

The authors declare no competing financial interest.

Corresponding authors Correspondence and material requests should be addressed to Dominique Gagliardi or Heike Lange.

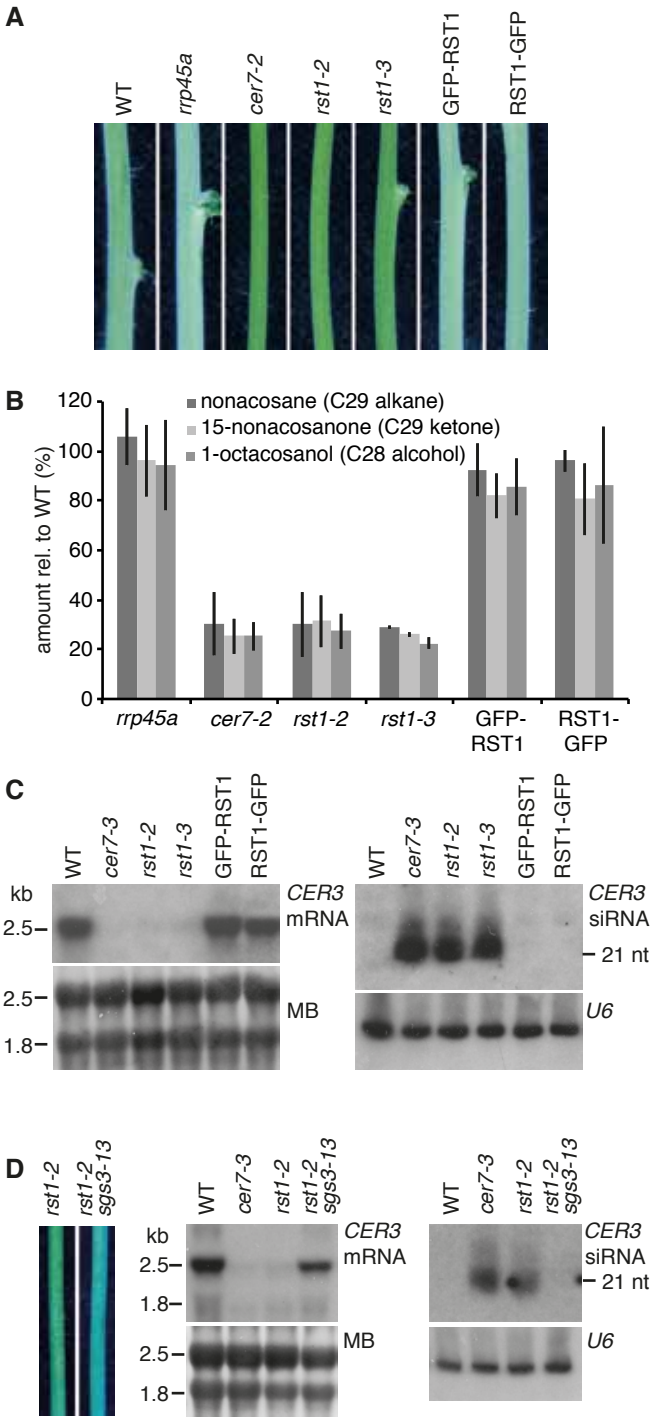

Fig. 1 The wax-deficient phenotype of *rst1* mutants is caused by silencing of the *CER3* gene. A. Inflorescence stems of *Arabidopsis* plants of the indicated genotypes. GFP-RST1 and RST1-GFP are *rst1-3* plants ectopically expressing RST1 fused to GFP. The whitish appearance of wild type stems is due to a layer of epicuticular wax deposited on the stem surface, while wax-deficient stems appear green and glossy. To better visualize the difference between normal and glossy stems, the white balance of the photograph was set to cold light (3800K), which accounts for the bluish appearance of the picture. **B**. Relative amounts of major stem wax compounds extracted from *Arabidopsis* stem sections. The barplot shows the mean of three replicates, error bars show the SD. **C**. Levels of *CER3* mRNA and *CER3*-derived siRNA in WT, *cer7* and *rst1* mutants. Total RNA extracted from stem samples of the indicated genotypes was separated by denaturing agarose (left) or polyacrylamide (right) electrophoresis, transferred to membranes and hybridised with a probe specific to *CER3*. The methylene blue (MB) stained membrane and hybridisation with a probe specific to *U6* snRNA are shown as loading controls, respectively. **D.** Mutating *SGS3* restores the wax phenotype of *rst1* mutants. Stem sections from *rst1-2* and *rst1-2 sgs3-13* plants are shown on the left. RNA blots show full-length *CER3* mRNA (mid) and *CER3*-derived siRNAs (right) in RNA samples extracted from stems of the indicated genotypes.

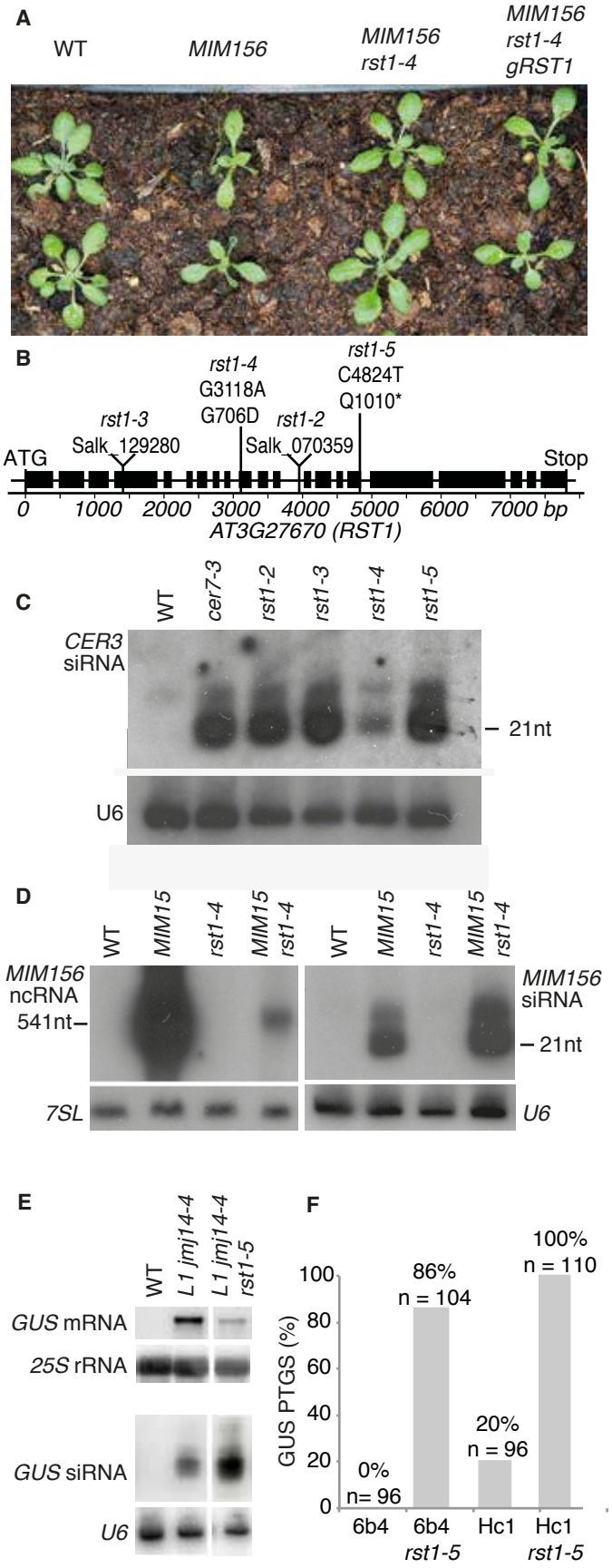

Fig. 2 RST1 suppresses silencing of transgenes. A. The *rst1-4* mutation suppresses the developmental phenotype induced by a *MIM156* transgene. **B.** Diagram of the *AT3G27670* gene encoding the RST1 protein. Boxes represent exons, lines represent introns. Triangles indicate the position of the T-DNA insertions in *rst1-2* and *rst1-3* lines. Vertical lines indicate the point mutations in *rst1-4* and *rst1-5*. **C.** *rst1-4* is a weak allele. Accumulation of *CER3*-derived siRNAs in wild type (WT), *cer7-3* and the four *rst1* alleles used in this study shown by a small RNA blot hybridised with a probe specific to *CER3*. **D**. RNA blots showing the accumulation of the full-length *MIM156* ncRNA and *MIM156*-derived siRNAs visualized by hybridisation with a probe specific to the *IPS1* backbone of the *MIM156* transgene. *7SL* RNA and *U6* snRNA are shown as loading controls. **E.** RNA blots showing that the *rst1-5* mutation results in reduced levels of the *GUS* mRNA and increased levels of *GUS*-derived siRNAs in the *L1 jmj14-4* background. *25S* rRNA and *U6* snRNA are shown as loading controls **F.** The *rst1-5* mutation increases S-PTGS frequency in both 6b4 and Hc1 reporter lines. The barplot shows the proportion of plants with silenced GUS expression in the indicated genotypes.

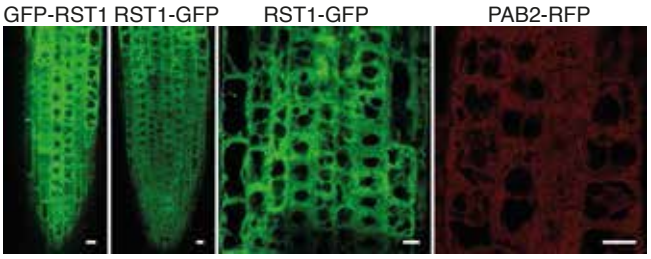

Fig. 3 RST1 is a cytosolic protein. Confocal microscopy of root tips from *Arabidopsis rst1-3* plants ectopically expressing GFP-RST1 and RST1-GFP fusion proteins. Poly(A) binding protein 2 (PAB2) fused to RFP is shown as cytosolic marker. Scale bars are 10 µm.

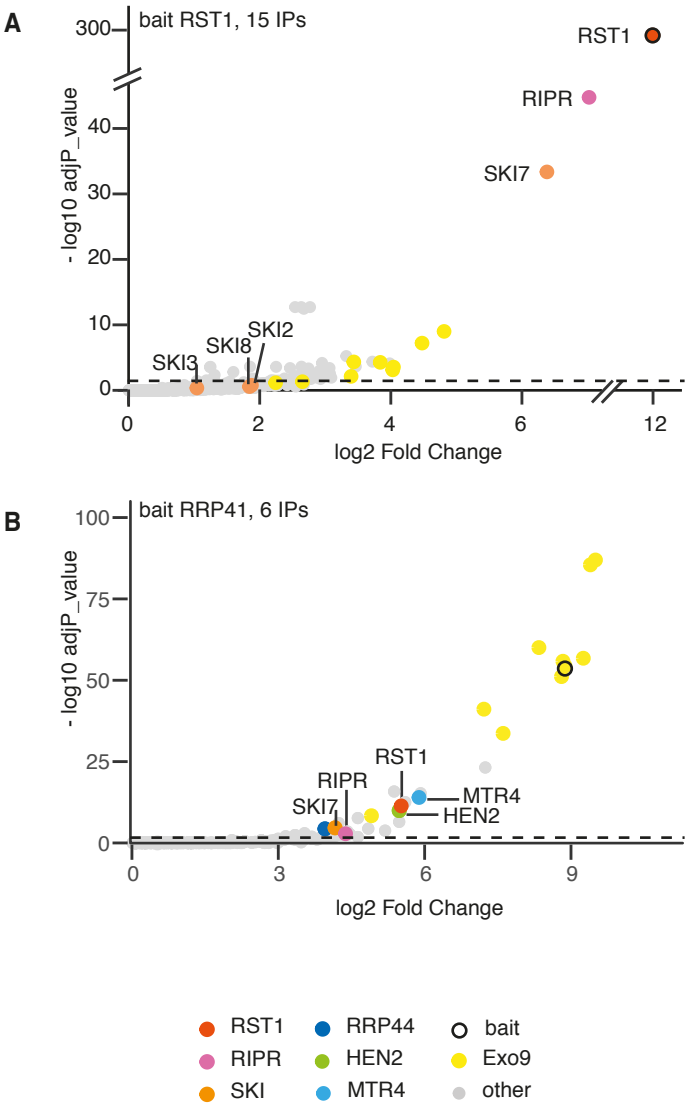

Fig. 4 RST1 co-purifies with the exosome, SKI7 and RIPR. Volcano plots show the enrichment of proteins co-purified with GFP-tagged RST1 (**A**) or RRP41 (**B**) as compared to control IPs. Y- and X-axis display adjusted p-values and fold changes, respectively. Note that nuclear exosome cofactors such as HEN2 and MTR4 are co-purified with RRP41 but not with RST1 as bait.

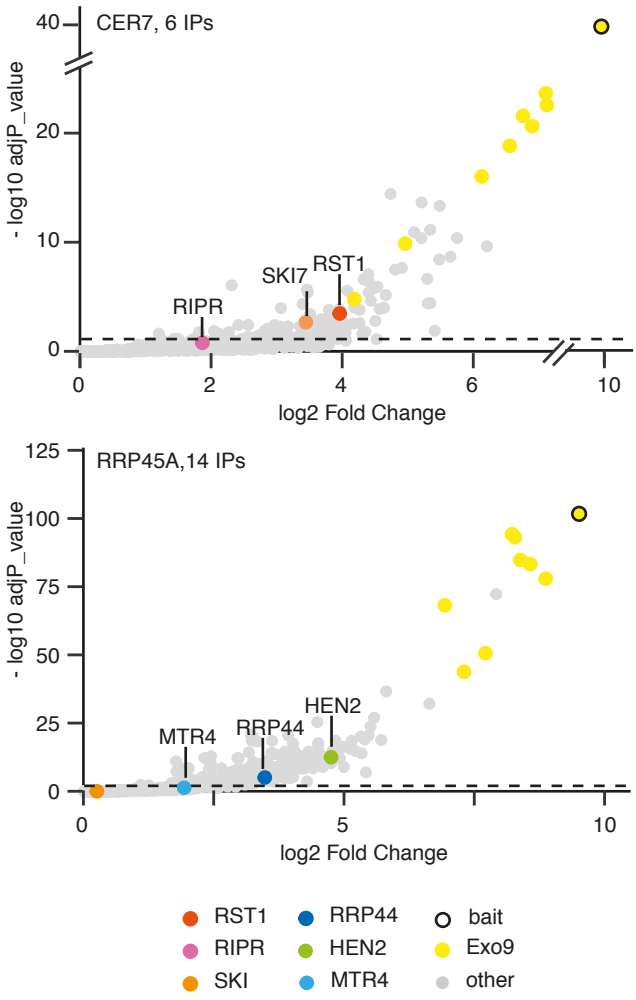

Fig. 5 RST1 and RIPR are bound to CER7-containing exosomes. Volcano plots show the enrichment of proteins co-purified with GFP-tagged RRP45B/CER7 (**A**) or RRP45A (**B**) as compared to control IPs. Y- and X-axis display adjusted p-value and fold change, respectively.

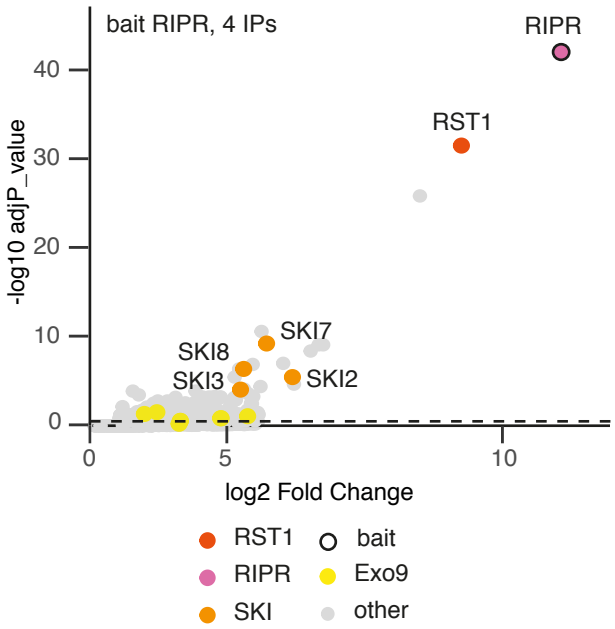

Fig. 6 RIPR co-immunoprecipitates RST1, SKI7 and the Ski complex. The Volcano plot shows the enrichment of proteins co-purified with GFP-tagged RIPR as compared to control IPs. Y- and X-axis display adjusted p-value and fold change, respectively.

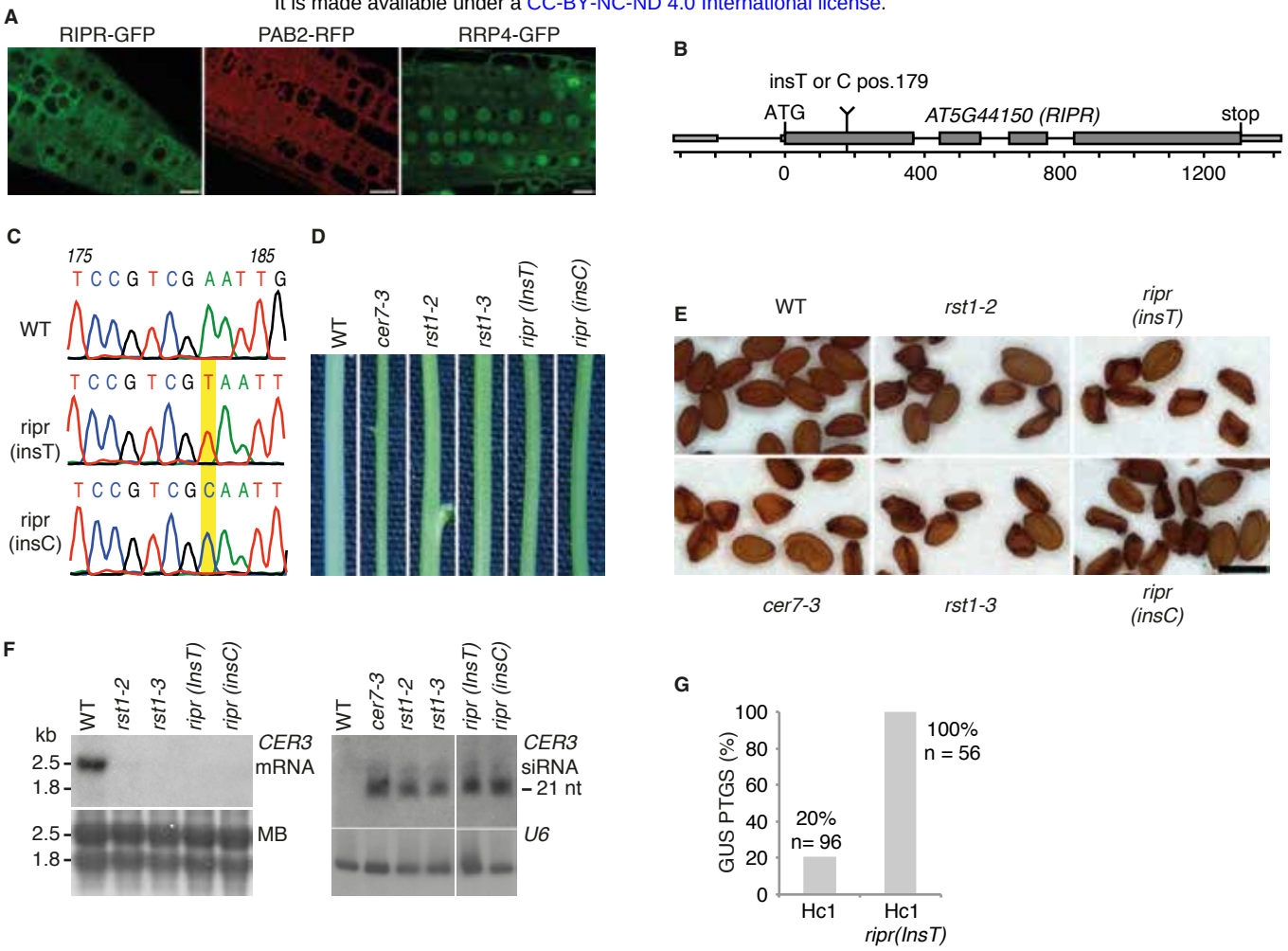

Fig. 7 Loss of RIPR function phenocopies *rst1* mutants. A. Confocal microscopy of plants expressing RIPR-GFP, the cytosolic marker PAB2-RFP and a GFP-tagged version of the exosome subunit RRP4. Scale bars are 20 µm. **B.** Scheme of the *AT5G44150* gene encoding the RIPR protein. Small and large boxes represent exons in the UTRs and CDS, respectively, lines represent introns. The single insertion of a T or C nucleotide at position 179 (from the ATG) results in a frameshift and creates a premature stop codon. **C.** Electrospherograms of the genomic DNA sequence surrounding the relevant position of the *AT5G44150* locus in wild type, *ripr(insT)* and *ripr(insC)* plants. **D.** Stem sections from wild type (WT), *cer7*, *rst1* and *ripr* plants. **E.** *cer7-3*, *rst1* and *ripr* mutants produce similar proportions of non-viable seeds. Scale bar is 0.5 mm. **F.** Northern blots showing the downregulation of the *CER3* mRNA (left) and the upregulation of *CER3*-derived siRNAs (right) in *ripr* mutants. Loading controls show the methylene blue stained membrane (MB, left) and the hybridisation with a probe specific to *U6* snRNA (right). **G.** RIPR is a silencing suppressor. The barplot shows the percentage of plants that spontaneously trigger silencing of the *Hc1 35S prom:GUS* S-PTGS reporter.

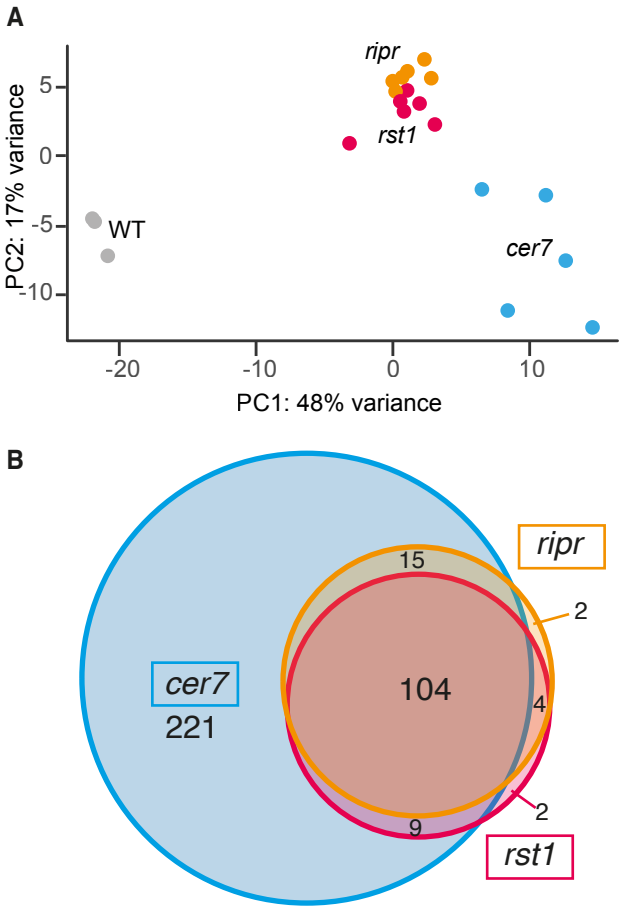

Fig. 8 Loss of RST1 or RIPR results in the accumulation of small RNAs that are also produced in *cer7* mutants A. Multidimensional scaling plot illustrating global variance and similarities between the 21/22 nt small RNA populations detected in the replicates of WT, *cer7*, *rst1* and *ripr*. **B.** Venn diagram showing that *rst1* and *ripr* mutants accumulate quasi identical populations of small RNAs almost all of which are also detected in *cer7* mutants.

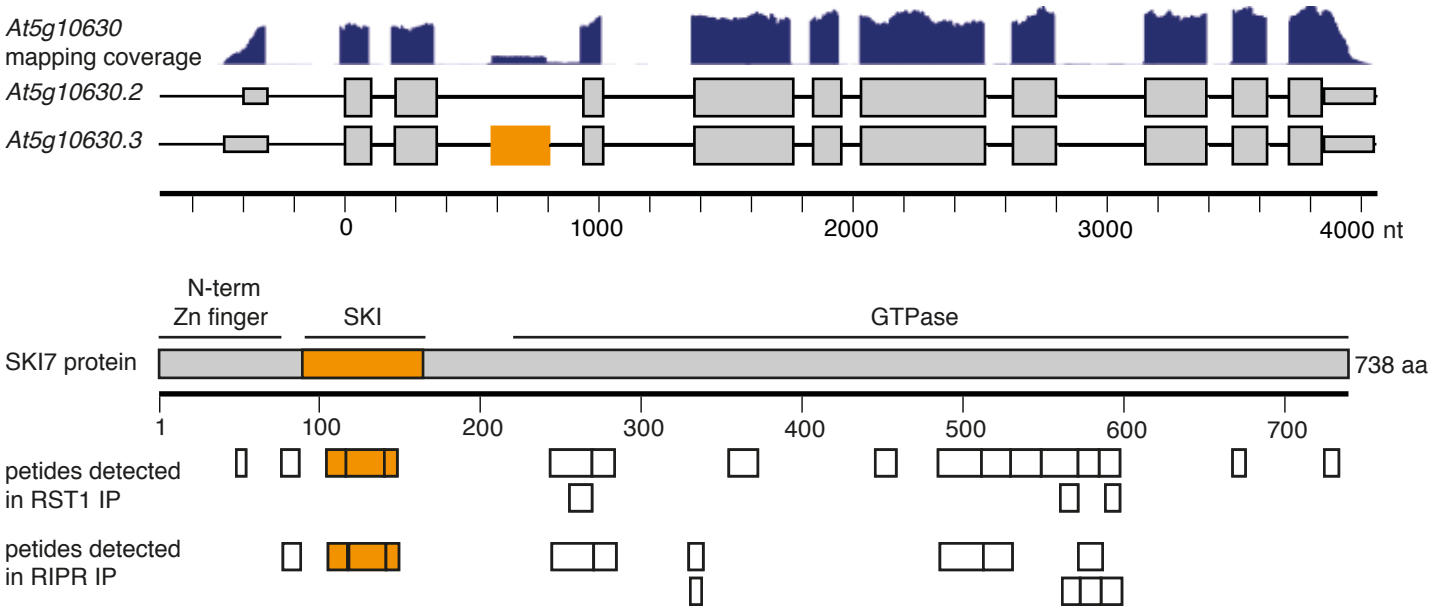

Supplementary Fig. 1 SKI7-specific peptides detected in RST1 and RIPR IPs. The top panel illustrates the mapping coverage (RNA seq data from light grown seedlings, source Araport11) of the *AT5G10630* locus and two (of five) gene models *AT5G10630.1* and *AT5G10630.4* encoding HBS1 and SKI7 proteins, respectively. Lines represent introns, small boxes represent 3' and 5' UTRs, large boxes represent exons. The exon specific to the SKI7- encoding mRNA is shown in orange. The lower panel illustrates the Arabidopsis SKI7 protein composed of an N-terminal and a Zn-finger domain thought to mediate the interaction with the SKI complex, the SKI7-specific domain encoded by the SKI7-specific exon and thought to be involved in recruitment of the exosome (in orange), and the large GTPase domain. The boxes below the diagram indicate unique peptides identified in the RST1 co-immunoprecipitation experiments with the SKI7-specific peptides again highlighted in orange.

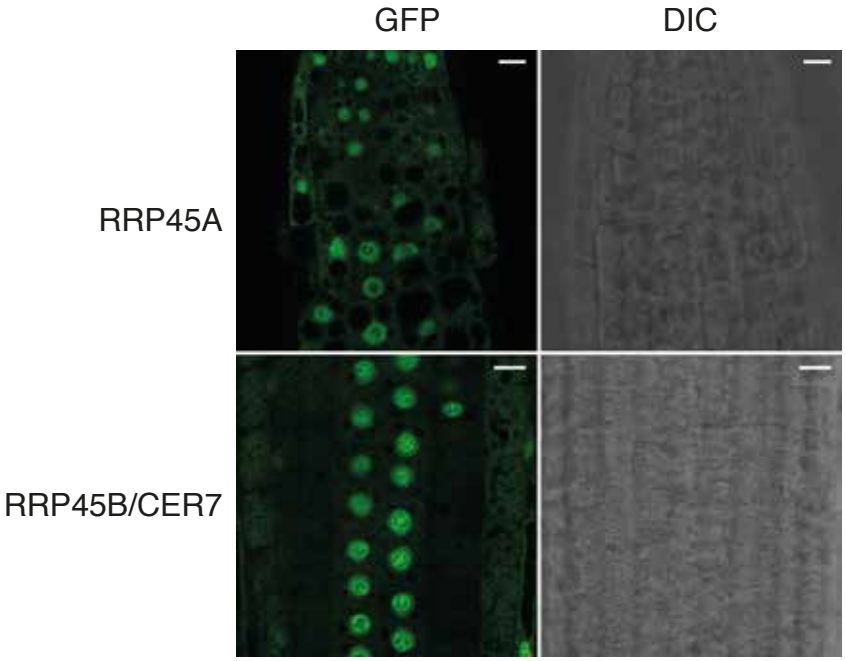

Supplementary Fig. 2 RRP45A and RRP45B/CER7 exosome subunits show similar intracellular distributions. Confocal microscopy images of *Arabidopsis* roots expression RRP45A (top) or RRP45B/CER7 (bottom) GFP fusion proteins. DIC, differential interference contrast. Scalebars are 10μm.

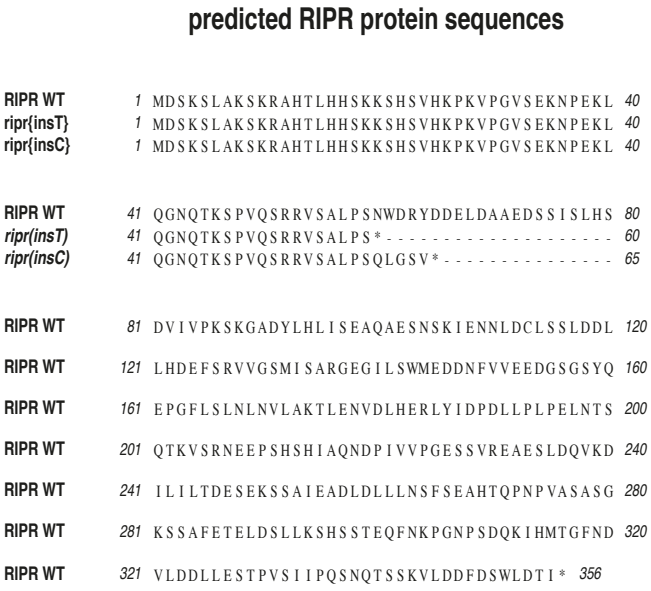

Supplementary Fig. 3 Frameshift mutations in *ripr(insT)* and *ripr(insC)* prevent the synthesis of full-length RIPR proteins.

Fig. 1A

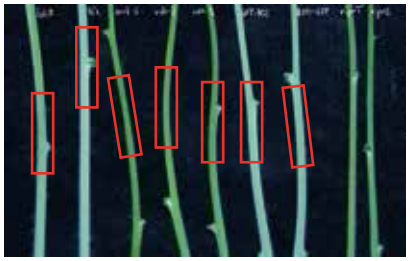

Fig. 1C HMW

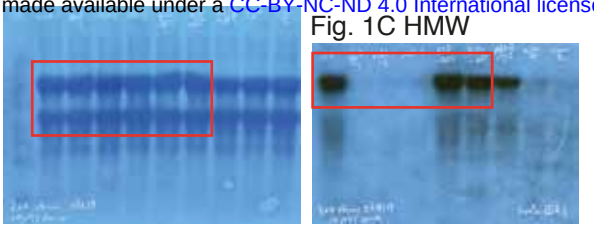

Fig. 2A

Fig. 1D

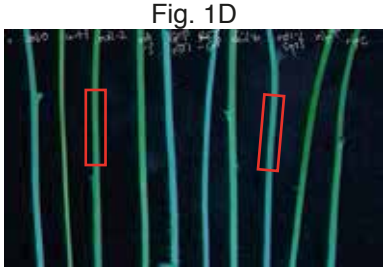

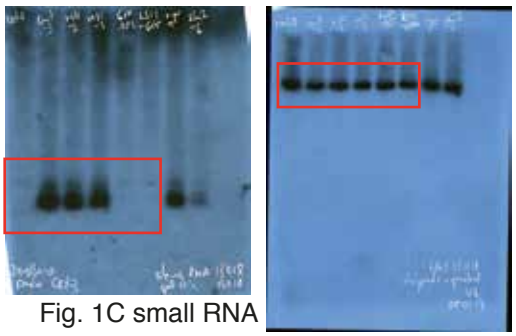

Fig. 1C small RNA

Fig. 2C

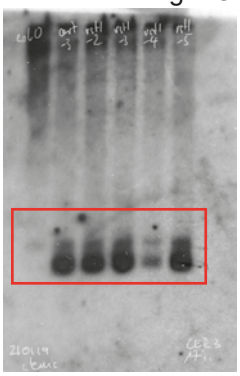

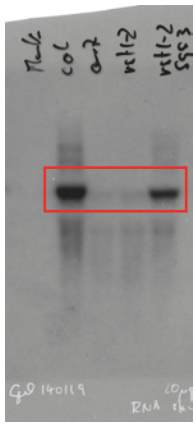

Fig. 1D HMW

Fig. 1D small RNA

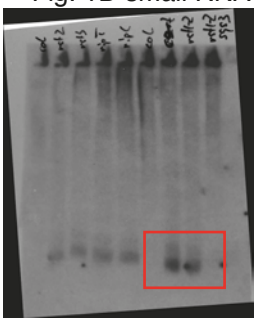

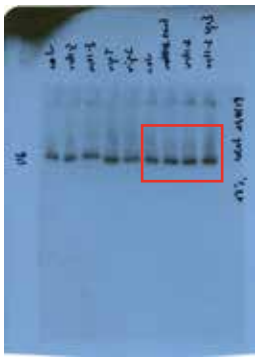

Fig. 7D

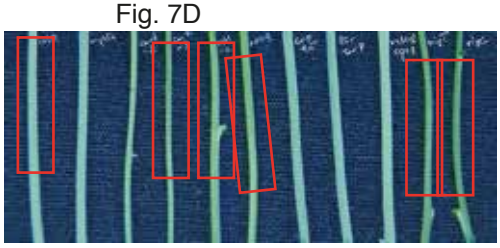

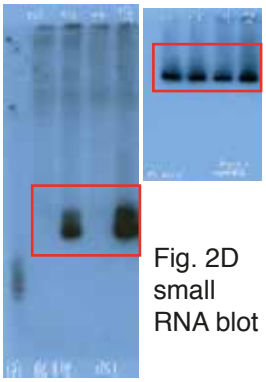

Fig. 2D small RNA blot

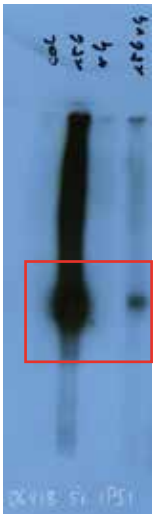

Fig. 2D LMW, MIM156

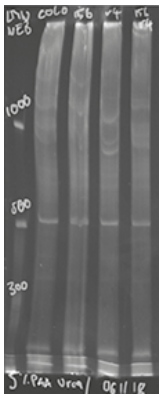

Fig. 2D EtBr

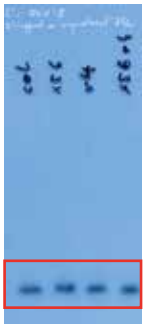

Fig. 2D LMW, U6

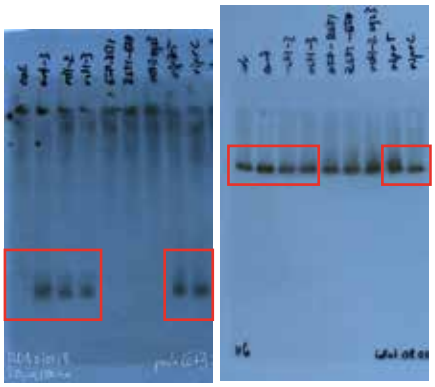

Fig. 7F small RNA blot

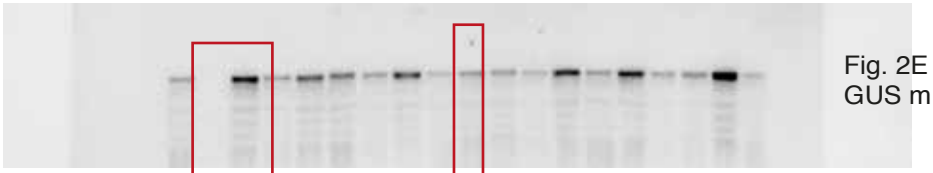

Fig. 2E GUS mRNA

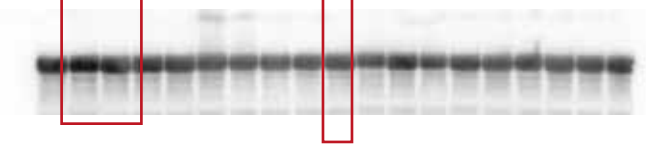

Fig. 2E 25S rRNA

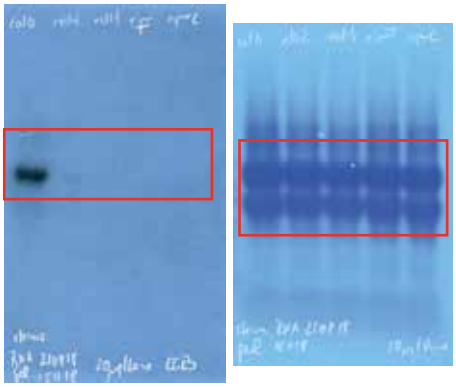

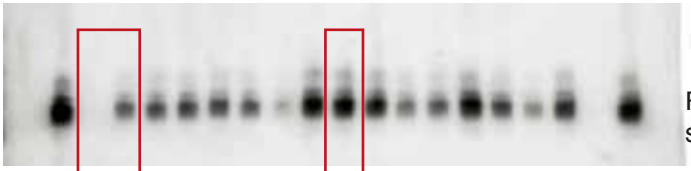

Fig. 2E small RNA GUS

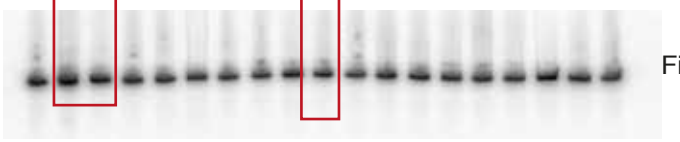

Fig. 2E, U6

Fig. 7F HMW

Supplementary Fig. 4 Uncropped images

Supplementary Table 6: Primers used in this study

Genotyping primers	
cer7-2 fw	ATATTTGAGTGGTGCTGCTGG
cer7-2 rev	AAACTCGACAAAGAGGGAAGC
cer7-3 fw	AAAGCTTCCCTCTTTGTCGAG
cer7-3 rev	GCCATTGGCATTAACTGTCAC
rrp45a fw	GTTGTTGGTTGCAGAGAAAGC
rrp45a rev	TGCGAGAAGTCTCAACATGTC
rst1-2 fw	GCGTGTTCTAAGCCATCTTTG
rst1-2 rev	GCAAGGAAATAAGAGCAAGGG
rst1-3 fw	TTGATTTCATCAATGGCTTCC
rst1-3 rev	CTGACAAGGGACGTTAGTTCG
rst1-4 fw	TGAGGTGTCTGAAGTGGTGCA
rst1-4 rev	CAAAGATGGCTTAGAACACGC, cleave product with *Ban1*
riprT/C fw	CGATGGACTCAAAATCTCTAGCTAAATCGAAGA
ripT/C rev	ACCTTGCCCGAACAACAAGA
sgs3-13 fw	AAGGCCATGCTTGTACATGAG
sgs3-13 rev	TATGAGGCTCTTAGAGCACGC
MIM156 fw	AAGAAAAATGGCCATCCCCTAGC
MIM156 rev	TGACAGAAGATAGAAGTGAGCAT
gRST1 fw	GACGTGTTGATTGAGATAGT
gRST1 rev	AACAGCTATGACCAT (M13 rev present in T-DNA)
probes	
CER3 fw	ACAGGTAATCTCAACTCCGAGG
CER3 rev	TGGAACACCAGCTACGACAC
IPS1 (MIM) fw	AAGAAAAATGGCCATCCCCTAGC
IPS1 (MIM) rev	TAGAGGGAGATAAACAAAACTCGCAGT
U6	GCTAATCTTCTCTGTATCGTTCCA
7SL	ATATGAAGATCGGACCAGCAGGC